Cocaine Analogue Conjugated Magnetic Nanoparticles for Labeling and Imaging Dopaminergic Neurons

SCHOLARONE™
Manuscripts

Cocaine Analogue Conjugated Magnetic Nanoparticles for Labeling and Imaging Dopaminergic Neurons

Mike Jeon[1], Guanyou Lin[1], Zachary R. Stephen[1], Josey E. Vechey[1], Manjot Singh[1], Richard Revia[1], Amy Hauck Newman[2], Diana Martinez[3], and Miqin Zhang[1]*

M. Jeon, G. Lin, Z. R. Stephen, J. E. Vechey, M. Singh, R. Revia, Prof. M. Zhang
[1]Department of Material Sciences and Engineering, University of Washington
Seattle, WA, 98195, USA
E-mail: mzhang@uw.edu

Dr. Amy Hauck Newman
[2]Medicinal Chemistry Section, Molecular Targets and Medication Discovery Branch
National Institute on Drug Abuse-Intramural Research Program
National Institutes of Health
333 Cassell Dr.
Baltimore, MD 21224

Prof. Diana Martinez, MD
[3]Department of Psychiatry, Columbia University Irving Medical Center
1051 Riverside Drive #66
New York, NY, 10032, USA
E-mail: dm437@cumc.columbia.edu

Abstract

Molecular imaging of the dopamine transporter (DAT) with Positron Emission Tomography (PET) or Single Photon Emission Computed Tomography (SPECT) has been widely used in studies of neurological and psychiatric disorders. Nevertheless, there is a great interest in expanding molecular imaging to include magnetic resonance technology, because of the superior spatial resolution this technology may provide. Here we present a magnetic nanoparticle (NP) that specifically targets dopaminergic neurons and allows DAT imaging with magnetic resonance imaging (MRI). The nanoparticle (namely, NP-DN) is composed of an iron oxide core and a polyethylene glycol (PEG) coating to which a DAT specific dopaminergic neurolabeler (DN) is conjugated. NP-DN displayed long-term stability with favorable hydrodynamic size and surface charge suitable for in vivo application. In vitro studies showed NP-DN was non-toxic, displayed specificity towards DAT-expressing neurons, and demonstrated a 3-fold increase in DAT labeling over non-targeted NP. Our study shows NP-DN provides excellent contrast enhancement for MRI and demonstrates great potential for neuroimaging.

1. Introduction

Molecular neuro-imaging has emerged as a powerful non-invasive method for pre-clinical and clinical investigation of neurological disorders arising from impaired dopamine (DA) signaling. The DA transporter (DAT) is a presynaptic membrane-spanning protein present in dopaminergic neurons and plays a critical role in regulating DA levels by recycling extracellular DA from the synapse to the cytosol. Studies have indicated DAT deficiency as a primary cause of aberrant DA regulation, which has been implicated in a number of neurological disorders including Parkinson's disease (PD), schizophrenia, attention deficit hyperactivity disorder, substance use disorders, and major depression.[1-3] Advancements in the molecular neuro-imaging of DAT have aided researchers in unraveling the underlying neuropathology of these various brain disorders. Clinically, DAT imaging has primarily shown utility in early diagnosis of PD and differentiation of PD from other non-degenerative parkinsonian disorders, with potential as a progressive biomarker in longitudinal studies.[2, 4] Despite clinical relevance, many in vivo DAT imaging applications are hindered by the limitations of currently available imaging probes and imaging modalities.

Current in vivo DAT imaging methods rely on Single Photon Emission Computed Tomography (SPECT) or Positron Emission Tomography (PET) utilizing a radiotracer composed of radionuclides bound to DAT-selective cocaine analogues.[2] Clinically relevant radiotracers include [^{123}I]FP-CIT and [^{123}I]β-CIT for SPECT imaging, and [^{18}F]FP-CIT and [^{11}C]RTI-32 for PET imaging.[2] The use of radiotracers, however, creates inherent limitations in radionuclide-based imaging. Radiotracers have short half-lives; [^{11}C], [^{18}F], and [^{123}I] possess half-lives of approximately 20 min, 110 min, and 13 hr respectively, constraining the imaging window post

administration.[5] Moreover, the chemistry associated with labeling DAT ligands with radionuclides can be challenging, and the short half-lives often necessitate on-site synthesis, limiting available facilities capable of carrying out these imaging methods. Despite their high sensitivity, radionuclide-based imaging also has inherently suboptimal spatial and temporal resolution and lack anatomical details, limiting the information that can be gained from these modalities.

Fluorescent probes and quantum dots have also been researched to visualize live neurons. Quantum dots with DAT-specific ligand have demonstrated the ability to detect DAT in transfected mammalian cells.[6, 7] Various fluorescent assays have been developed to monitor DAT expression, function, and plasma membrane trafficking. Although fluorescent probes and quantum dots offer superior spatial and temporal resolution compared to PET and SPECT,[7] they are inherently limited by poor penetration depth, restricting their use to in vitro and small animal studies.

The limitations of the-above neuro-imaging modalities prompt the need to develop a better imaging platform that can address some or all these limitations. The application of magnetic resonance imaging (MRI) to dopaminergic neuron imaging may provide a new approach for clinical research on neuro-psychiatric disorders. MRI is a ubiquitous, noninvasive technique that provides excellent spatial resolution and great penetration depth, and able to image opaque objects. MRI contrast agents, especially superparamagnetic iron oxide nanoparticles (SPIONs), have the potential to allow for MRI-based molecular imaging. SPIONs as MRI contrast agents have been extensively investigated for imaging and trafficking of various cells, such as brain tumor cells for cancer diagnosis,[8-10] stem cells in cardiac cell therapy,[11] and phagocytic cells in inflammatory diseases.[12] These studies demonstrated SPIONs have excellent MRI contrast enhancement, long blood circulation time in vivo, high spatial resolution, and good biocompatibility. Despite these

encouraging advances, little work has been done in the use of SPIONs as contrast agent for MRI in imaging neurons. This is largely due to a lack of DAT-specific ligand molecules and the high hydrophobicity of DAT-specific molecules that are incompatible with aqueous biological fluids.

Here we report the development of an iron oxide nanoparticle capable of labeling live dopaminergic neurons and providing contrast for MRI. The nanoparticle consists of a superparamagnetic iron oxide core coated with poly(ethylene) glycol (PEG), and subsequently labeled with dopaminergic neurolabeler (DN, NP-DN) and Cy5 fluorophore (NP-DN-Cy5). The small core size of iron oxide (<10 nm) ensures high cellular uptake in vitro and a good pharmacokinetic profile for in vivo applications. Polyethylene glycol (PEG) serves as a stabilizer that prevents particle aggregation. The DN used in this study is from the 3-phenyltropane class of DAT inhibitors with modification to the tropane ring to provide high DAT affinity.[13] We characterized the morphology, size distribution, zeta potential, and stability of these nanoparticles with transmission electron microscopy (TEM) and dynamic light scattering (DLS). We used UV-vis spectroscopy to quantify Cy5 and DN on the nanoparticles. The targeting efficacy was assessed using flow cytometry, and the labeling was monitored using confocal fluorescence microscopy. Targeting specificity of NP-DN was also evaluated in human DAT expressing cell line, EM4-hDAT (positive control, DAT$^+$), and null-transfected EM4 cells (negative control, DAT$^-$) using in vitro MR imaging. The viability of the two cell lines after treatment was evaluated using the Alamar Blue assay.

2. Experimental

Materials: All chemicals were purchased from Sigma-Aldrich (St. Louis, MO, USA) with the following exceptions: 3-(triethoxysilyl)propyl succinic anhydride (SATES) from Gelest

(Arlington, VA, USA); 2000 MW mono-amine functionalized poly(ethylene) glycol (mPEG$_{2K}$-NH$_2$) from Laysan Bio (Arab, AL, USA); Cyanine5 NHS ester from Lumiprobe (Hallandale Beach, FL, USA); NHS-PEG$_{12}$-maleimide and succinimidyl 3-(2-pyridyldithio)propionate (SPDP) from Pierce Biotechnology (Rockford, IL, USA).

Modification of DN: DN was synthesized in the Medicinal Chemistry Section at the NIDA-Intramural Research Program by Dr. Mu-Fa Zou, following a previously published procedure.[13] DN was thiolated via SPDP activation and reduction via TCEP. 1 mg of DN was reacted with 0.98 mg of succinimidyl 3-(2-pyridyldithio)propionate (SPDP) in 100 μL DMSO with 2% N,N-diisopropylethylamine (DIPEA). The solution was reacted for 48 hours at room temperature. The SPDP-activated DN was then reduced by reaction for 30 minutes with an excess of tris(2-carboxyethyl)phosphine hydrochloride (TCEP) (4 mg TCEP in 100 μL thiolation buffer, pH = 8.5).

NP synthesis and conjugation of Cy5 and DN: 8 nm oleic acid coated iron oxide particles were synthesized and coated with PEG following the reported procedures.[14, 15] Cy5 was conjugated directly onto the NPs, while DN was conjugated via a heterobifunctional PEG crosslinker. To create NP-Cy5, 2 mg of NP was reacted with Cy5 NHS ester (0.1 mg in 10 μL DMSO) in 1 mL 0.1 M NaHCO$_3$ buffer (pH 8.5) for 1 hour at room temperature. The excess Cy5 was removed via S-200 sephacryl resin equilibrated with deionized water. One mg of NP-Cy5 was then reacted with 0.926 mg of NHS-PEG$_{12}$-maleimide (sm(PEG)$_{12}$) in 1 mL 0.1 M NaHCO$_3$ buffer (pH 8.5) for 30 minutes at room temperature. The excess crosslinker was removed with a zeba spin column equilibrated in deionized water. The product was collected and split in two equal portions. The control NPs were synthesized by reacting with excess hydrolyzed Traut's reagent, while targeted

NPs were synthesized by reacting with 0.2 mg DN-SH (dissolved in 20 µL DMSO). After overnight rocking, the particles were purified with an S-200 column equilibrated into deionized water.

Physicochemical characterization of NP: The core size and morphology were determined via TEM images obtained using an FEI TECNAI F20 TEM (Hillsboro, OR). The core diameters were analyzed using Image J to obtain average size and standard deviation. Hydrodynamic size, stability, and zeta potential were obtained using a DTS Zetasizer Nano (Malvern Instruments, Worcestershire, UK). DLS samples were prepared at 50 µg Fe/mL. Hydrodynamic size distribution was obtained in PBS, biological stability was analyzed in DMEM with 10% FBS and 1% antibiotic-antimycotic, and zeta potential was measured in 20 mM HEPES, pH = 7.4.

Quantification of Cy5 on NP: The number of Cy5 molecules per NP was determined using UV-vis spectroscopy. Samples of NP and NP-Cy5 were analyzed at a concentration of 10 µg/ml. The spectrum of NP was subtracted from the spectrum of NP-Cy5, to properly blank the system. The absorbance at 646 nm, along with Cy5's extinction coefficient of 271,000 $L \cdot mol^{-1} \cdot cm^{-1}$, was used to determine the molar ratio of Cy5:NP.

Chemical analysis by FTIR: FTIR spectra of DN, NP-TR, and NP-DN were obtained using a Nicolet 6700 spectrometer (Thermo Scientific Inc., Waltham, MA) at 4 cm^{-1} resolution and the signal was averaged over 64 scans. The samples were freeze-dried and ground with a mortar and pestle to a fine powder. The powder was pressed into a pellet with KBr for analysis.

Quantification of DN per NP: The number of DN molecules per NP was determined using UV-vis spectroscopy. Samples of NP-TR and NP-DN were analyzed at a NP concentration of 10 µg/ml.

Additionally, standards of DN at 0–50 µg/ml in DMSO were analyzed at 275 nm, and the absorbance values were used to produce a standard curve. The difference in absorbance at 275 nm between the spectrum of NP-DN and the spectrum of NP-TR was calculated and fitted onto the standard curve. The molar ratio of DN:NP was evaluated to be ~137 DN/NP.

Viability of cells treated with NPs: Cells were seeded in a 96-well plate (2,000 cells per well) and incubated overnight. Cells were incubated with NP-TR and NP-DN at equivalent iron concentrations of 0–100 µg Fe/ml for 24 or 72 hours. Alamar Blue reagent (Invitrogen, Carlsbad, CA) was added and incubated for 2 hours following the manufacturer's instruction. A microplate reader (Spectra i3, Molecular Devices, Sunnyvale, CA) was used to measure the fluorescence at 550 nm excitation and 590 nm emission.

Assessment of NP targeting: EM4 and EM4-hDAT cells were seeded onto 24-well plates (125,000 cells per well) and incubated overnight. Cells were then incubated with NPs at 50 µg/ml for 30 minutes at 37°C, followed by washing thrice with PBS. Cells were trypsinized, fixed in 4% formaldehyde, washed and suspended in PBS. The samples were then analyzed by flow cytometry (FACSCanto, II, BD Biosciences).

Confocal fluorescence microscopy: Cells were plated on glass coverslips and attached overnight. Cells were then washed thrice in PBS and fixed in 4% formaldehyde for 0.5 hours at room temperature. Cells were washed thrice with PBS to remove the formaldehyde, and were stained with WGA-AF555 and DAPI. Coverslips were mounted on slides with Prolong Gold antifade solution (Invitrogen, Carlsbad, CA). Images were acquired on a LSM 510 Meta confocal fluorescence microscope (Carl Zeiss, Inc., Peabody, MA).

In vitro MR imaging: Quantitative T_2 MR imaging scan sequences were used to investigate the contrast enhancing capabilities of NP-DN. MR imaging was conducted on a Bruker Avance III 600 MHz, 14 T wide bore spectrometer. NP-DN in PBS were pipetted into glass vials (3.25 mm I.D., 5 mm O.D., 200 μL volume) at concentrations of 0–25 μg Fe/mL. The vials were fixed in place inside a water reservoir; the water served as a homogeneous background signal to minimize magnetic susceptibility variations near samples. The secured vials were placed in a 25-mm single-channel ^{1}H radiofrequency receiving coil (PB Micro 2.5). Quantitative T_2 values of NP-DN were obtained using a multi-spin multi-echo (MSME) pulse sequence with TR = 2500 ms, TE = 6.7 + 6n ms (n = 0–16), and 78×156 μm^2 in-plane resolution with 0.5 mm slice thickness for 14 slices. Analysis of MR imaging data was accomplished with the FMRIB software library (FSL), Paravision 5.1 analysis package (Bruker), and ImageJ (NIH). T_1 values were determined within a circular, 100-voxel region of interest. Similarly, cells at 250,000 cells/mL were incubated with NP-DN or NP-TR at 100 μg Fe/ml in compete medium for 2 hours. The cells were washed thrice with PBS and resuspended in 50 μL 0.5% agarose to fix the cells, which were analyzed in the same manner as described above.

Statistical analysis: Results are presented as mean values ± standard deviation from three independent experiments. Statistical significance was determined using Student's t-test (p < 0.0005) for flow cytometry), using OriginPro 8.0. All results from targeting experiments and cell viability assays were normalized to the untreated treatment group.

3. Results and Discussion

3.1 Synthesis and characterization of NPs

The base NP was synthesized and modified with PEG coatings as previously described.[15, 16] The base NP is composed of an iron oxide core that has shown to be an effective contrast agent for MRI in vitro and in vivo.[8, 17, 18] The PEG coating confers the NP colloidal stability in aqueous solutions and provide terminal amine groups for further chemical conjugation.

The dopaminergic neurolabeler (DN) was synthesized following published methods.[13] **Figure 1a** schematically illustrates the synthesis of NP-DN. DN was first thiolated via reaction with succinimidyl 3-(2-pyridyldithio) propionate (SPDP), followed by reduction with tris(2-carboxyethyl) phosphine hydrochloride (TCEP). Concurrently, the base NP was modified via a bifunctional PEG_{12}-crosslinker; the NHS-ester moiety of the PEG crosslinker was reacted with the amine-terminal-NP to form NP-mal. DN-SH was then reacted with the maleimide moiety of NP-mal to create NP-DN. Hydrolyzed Traut's reagent served as a dummy molecule for our non-targeted control NPs (NP-TR). **Figure 1b** shows a schematic representation of targeting and labeling of dopaminergic neurons by NP-DN.

The behavior and efficacy of NPs are dictated by their physicochemical properties. The core morphology and size play important roles: the former can affect cellular uptake due to the differences in cellular interaction, while the latter affects the magnetic properties of the iron oxide core.[19-21] TEM was used to assess the core size and morphology (**Figure 2a**). The iron oxide cores were spherical with an average diameter of 8 nm which falls within the appropriate size range to enable superparamagnetism.[22] Hydrodynamic size and zeta potential are important factors that influence NP interaction with physiological and cellular barriers. Dynamic light scattering (DLS) was used to obtain the hydrodynamic sizes and zeta potentials of NP, NP-TR, and NP-DN (**Figure 2b-d**). The NP had an average hydrodynamic size of 25.9 ± 0.59 nm with a polydispersity index of 0.084 in saline. The conjugation of ligand DN via bifunctional PEG_{12}-crosslinker to form NP-

DN increased the hydrodynamic size to 30.2 ± 1.25 nm. Similarly, conjugation of hydrolyzed Traut's reagent via the same crosslinker to form NP-TR (non-targeted control) increased the size to 29.1 ± 0.97 nm (**Figure 2b**). The addition of the PEG crosslinker is likely responsible for the increase in hydrodynamic size of NP-TR and NP-DN. Both NP-TR and NP-DN showed minimal growth in cell culture media (Dulbecco's modified Eagle's medium with 10% serum), demonstrating prolonged colloidal stability (**Figure 2d**). Both NPs remained their sizes within the optimal size range of 10–100 nm preferable for in vivo application, wherein they are large enough to avoid filtration by the kidneys, yet small enough to avoid elimination by the MPS. Zeta potential impacts nonspecific uptake by cells through charge interactions. The zeta potential of the NP was measured to be −8.78 ± 6.41 mV, while NP-TR and NP-DN have zeta potentials of −9.2 ± 4.72 and −9.23 ± 2.72 mV, respectively (**Figure 2c**). The negligible difference in zeta potential could be explained by the dense polymeric coating; the hydrophobic DN is burrowed within the coating causing negligible change to the zeta potential. The slightly negative to near neutral zeta potentials minimize electrostatic interaction with non-target cells and extracellular matrix. The physicochemical properties of NP, NP-TR, and NP-DN are summarized in **Table 1**.

The magnetic properties of NP-DN were evaluated by MRI to demonstrate the potential of NP-DN to serve as a MRI contrast agent (**Figure 3a-b**). The T_2 signal intensity increased with increasing NP (i.e., Fe) concentration, and the resulting $1/T_2$ (R_2) vs. Fe concentration plot shows a linear correlation, yielding a transverse relaxivity (slope of the curve) of 46.22 s^{-1} mM^{-1}, at 14 T field strength. The ability of NP-DN to provide significant negative contrast at low concentrations indicates its potential as a contrast agent for in vivo applications.

The conjugation of ligand DN was verified and quantified using FTIR and UV-vis spectroscopy, respectively. There are two FTIR peaks from DN: 1733 cm^{-1} from C=O stretching in the 2β-ester carbonyl attached to the tropane ring, and 668 cm^{-1} from C-Cl bonds in the 3β-3,4-dichloro-phenyl substituent (**Figure 4a**). These two peaks are not present in the FTIR spectrum for NP-TR, but they are present in the FTIR spectrum for NP-DN, indicating DN is successfully conjugated onto NP-DN. DN exhibits a broad peak centered approximately at 275 nm under UV-vis. (**Figure 4b**). The difference in absorbance of NP-TR (no DN) and NP-DN at 275 nm was used to calculate the amount of DN conjugated to NP-DN using Beer's Law. Quantitation results indicate NP-DN has ~137 DN molecules per NP. Despite the large number of hydrophobic DN molecules per NP, the conjugation of DN did not affect the stability of NP-DN in a biologically relevant solution (Figure 2d).

3.2 Cell viability of NP-DNs

It is common for small molecule targeting agents to be toxic due to their inherent hydrophobicity. Therefore, we tested the cell viability of both NP-TR and NP-DN on two cell lines: EM4 and EM4-hDAT. The EM4 cells are derived from the human embryonic kidney cell line, HEK 293, transfected with a macrophage embryonic receptor to increase their adherence to the tissue culture plastic, and were used as the host cells for stable expression of hDAT. EM4-hDAT cells express the DAT (positive control, DAT$^+$) while the EM4 cells are devoid of the DAT (negative control, DAT$^-$).[23-28]

The two cell lines were treated at various NP concentrations in cell culture media for 24 and 72 hours, and cell viability was evaluated using the Alamar Blue assay. **Figures 5a-b** show the viability of the DAT$^-$ cell line treated with either NP-TR or NP-DN of various concentrations

for 24 and 72 hours, respectively, while **Figures 5c-d** show the viability for the DAT$^+$ cell line at 24 and 72 hours, respectively. Both NP-TR and NP-DN were minimally cytotoxic, even at the highest NP concentration (100 μg Fe/ml) after 72 hours of incubation, highlighting the good biocompatibility of both NP-TR and NP-DN with dopaminergic neurons.

3.3 NP-DN targeting of DAT

The 3β-phenyltropane analogues of cocaine typically bind with high affinity to DAT. Indeed, the 3*β*-3,4-dichloro-phenyl ring substitution on the tropane ring (Figure 1a) results in subnanomolar DAT affinity.[13, 29] Furthermore, modification of this NP with fluorescent ligands such as rhodamine red or Cy3 via a short linking chain from the terminal amine of DN only minimally reduced DAT binding affinities of the resultant compounds[9,14] predicting potential success of the present nanoprobe design.

DAT$^+$ and DAT$^-$ cell lines were utilized to evaluate the targeting specificity of DN when bound to the NP surface. NPs were labeled with Cy5 fluorophore at a molar ratio of 2:1 for Cy5:NP. DAT$^+$ and DAT$^-$ cell lines were treated with equal amounts of NP-TR and NP-DN and incubated for 2 hours at 37°C. Following the incubation, the cells were washed thrice, fixed, and analyzed by flow cytometry (**Figure 6a-c**). NP-TR and NP-DN exhibited some nonspecific labeling of DAT$^-$ cells, but no significant difference was observed between NP-TR and NP-DN in the negative control cells (**Figure 6a**). The evaluation of NP-TR and NP-DN labeling of DAT$^+$ showed NP-TR produced similar labeling to that observed for the DAT$^-$ cells, while the NP-DN exhibited a nearly 300% increase in labeling in comparison to NP-TR when incubated with DAT$^+$ cells. This suggests that the NP-DN is capable of targeting and labeling DAT expressing neurons.

NP targeting of DAT was further examined by MRI to demonstrate the ability of NP-DN to label DAT expressing cells and provide contrast in MRI. DAT^+ and DAT^- cells were treated with equal amounts of NP-TR or NP-DN for 2 hours, suspended in agarose, and imaged with a 14 T MRI magnet (**Figure 6d**). The DAT^+ cell treated with NP-DN show considerably greater (negative) contrast than DAT^+ cells treated with NP-TR and DAT^- cells treated with either NP-DN or NP-TR. This suggests that NP-DN can specifically target neurons, and also serve as a contrast agent for MRI.

Confocal microscopy was also used to visualize NP-DN targeting of DAT. DAT^+ and DAT^- cells were incubated in cell culture media containing Cy5-labeled NP-TR or NP-DN at equal concentration for 2 hours (**Figure 7**). Cells were fixed and stained with DAPI and WGA-555 to show the nuclei (blue, first column) and membranes (red, second column), respectively. NPs in treated cells are shown green (third column). The overlay images (fourth column) indicate NP-DN specifically labels DAT^+ cells. Analysis of NP-DN labeling of DAT^+ cells by flow cytometry, MRI, and confocal microscopy all indicate NP-DN can target and label DAT expressing cells, provide contrast using a clinically relevant imaging modality, and thus can be used to effectively image dopaminergic neurons.

NP-DN imaging via MRI potentially offers a new method for neurologists to study various disorders associated with poor and/or irregular dopamine regulation. The increased resolution provided by MRI combined with a contrast agent with an imaging time scale not limited by the half-lives of currently employed DAT imaging radiotracers could provide crucial spatiotemporal insights on aberrant dopamine regulation in basic and translational research. For clinical uses of NP-DN, future studies will need to assess the ability of NP-DN to bypass biological barriers including the blood-brain barrier (BBB) in order to reach target cells within the brain. NP-DN

possess many favorable characteristics for improving the likelihood of success to reach the brain, including small size (~26 nm) and a PEG functional surface to minimize protein absorption and increase circulation time.[30] However, additional vasculature escape methods may need to be employed for NP-DN to reach its potential. These methods include exploitation of transport- and receptor-mediated transcytosis, the use of cell penetrating peptides for direct access to cells,[30, 31] and nanomaterial-induced endothelial leakiness[32, 33] which can be facilitated by magnetic targeting of NP-DN through disruption of adherens junctions and actin filaments.[34]

4. Conclusions

Iron oxide nanoparticles conjugated with a dopaminergic neuron targeting ligand, DN, were developed to label and image dopaminergic neurons. NP-DN showed high loading of DN while maintaining favorable characteristics for in vivo applications including excellent biocompatibility, long-term stability in cell culture media, good monodispersity, and a favorable hydrodynamic size. Cell viability assessment of NP-TR (non-targeted control) and NP-DN produced minimal toxicity. Flow cytometry analysis demonstrated that NP-DN exhibited a nearly 300% increase in labeling of EM4-hDAT (DAT$^+$) cells as compared to NP-TR. DAT$^+$ cells treated with NP-DN showed considerably greater MR contrast than cells treated with NP-TR. Confocal microscopy showed that DAT$^+$ cells treated with NP-DN yielded vastly higher labeling compared to NP-TR. These results demonstrated the great potential of NP-DN to successfully label and image neurons, taking a step forward in bringing MR-based neuroimaging to the clinical setting.

Acknowledgements

References

1. J. Seibyl, D. Jennings, R. Tabamo and K. Marek, *Minerva medica*, 2005, **96**, 353-364.
2. F. Ba and W. R. Martin, *Parkinsonism & related disorders*, 2015, **21**, 87-94.
3. J. L. Cummings, C. Henchcliffe, S. Schaier, T. Simuni, A. Waxman and P. Kemp, *Brain : a journal of neurology*, 2011, **134**, 3146-3166.
4. K. Ikeda, J. Ebina, K. Kawabe and Y. Iwasaki, *Intern Med*, 2019, **58**, 1665-1672.
5. P. W. Miller, N. J. Long, R. Vilar and A. D. Gee, *Angewandte Chemie International Edition*, 2008, **47**, 8998-9033.
6. J. Eriksen, S. G. Rasmussen, T. N. Rasmussen, C. B. Vaegter, J. H. Cha, M. F. Zou, A. H. Newman and U. Gether, *The Journal of neuroscience : the official journal of the Society for Neuroscience*, 2009, **29**, 6794-6808.
7. O. Kovtun, I. D. Tomlinson, D. S. Sakrikar, J. C. Chang, R. D. Blakely and S. J. Rosenthal, *ACS chemical neuroscience*, 2011, **2**, 370-378.
8. Z. R. Stephen, F. M. Kievit, O. Veiseh, P. A. Chiarelli, C. Fang, K. Wang, S. J. Hatzinger, R. G. Ellenbogen, J. R. Silber and M. Zhang, *ACS Nano*, 2014, **8**, 10383-10395.
9. Z. R. Stephen, P. A. Chiarelli, R. A. Revia, K. Wang, F. Kievit, C. Dayringer, M. Jeon, R. Ellenbogen and M. Zhang, *Cancer Res*, 2019, **79**, 4776-4786.
10. O. Veiseh, C. Sun, C. Fang, N. Bhattarai, J. Gunn, F. Kievit, K. Du, B. Pullar, D. Lee, R. G. Ellenbogen, J. Olson and M. Zhang, *Cancer Res*, 2009, **69**, 6200-6207.
11. M. R. Santoso and P. C. Yang, *Stem Cells Int*, 2016, **2016**, 4198790.
12. V. Hubert, C. Dumot, E. Ong, C. Amaz, E. Canet-Soulas, F. Chauveau and M. Wiart, *Sci Rep*, 2019, **9**, 10046.
13. J. H. Cha, M.-F. Zou, E. M. Adkins, S. G. F. Rasmussen, C. J. Loland, B. Schoenenberger, U. Gether and A. H. Newman, *Journal of Medicinal Chemistry*, 2005, **48**, 7513-7516.
14. J. A. Park, K.; Hwang, Y.; Park, J.-G.; Noh, H.-J.; Kim, J.-Y.; Park, J.-H.; Hwang, N.-M.; Hyeon, T, *Nat. Mater.*, 2004, **3**, 891.
15. C. Fang, N. Bhattarai, C. Sun and M. Zhang, *Small (Weinheim an der Bergstrasse, Germany)*, 2009, **5**, 1637-1641.
16. Q. Mu, M. Jeon, M. H. Hsiao, V. K. Patton, K. Wang, O. W. Press and M. Zhang, *Advanced healthcare materials*, 2015, **4**, 1236-1245.
17. P. A. Chiarelli, R. A. Revia, Z. R. Stephen, K. Wang, M. Jeon, V. Nelson, F. M. Kievit, J. Sham, R. G. Ellenbogen, H. P. Kiem and M. Zhang, *ACS Nano*, 2017, **11**, 9514-9524.
18. Z. R. Stephen, R. N. Gebhart, M. Jeon, A. A. Blair, R. G. Ellenbogen, J. R. Silber and M. Zhang, *Bioconjug Chem*, 2017, **28**, 194-202.
19. X. Huang, X. Teng, D. Chen, F. Tang and J. He, *Biomaterials*, 2010, **31**, 438-448.

20. Y. Jiang, S. Huo, T. Mizuhara, R. Das, Y. W. Lee, S. Hou, D. F. Moyano, B. Duncan, X. J. Liang and V. M. Rotello, *ACS nano*, 2015, **9**, 9986-9993.

21. N. P. Truong, M. R. Whittaker, C. W. Mak and T. P. Davis, *Expert opinion on drug delivery*, 2015, **12**, 129-142.

22. R. A. Revia and M. Zhang, *Mater Today (Kidlington)*, 2016, **19**, 157-168.

23. S. U. Park, J. V. Ferrer, J. A. Javitch and D. M. Kuhn, *The Journal of Neuroscience*, 2002, **22**, 4399-4405.

24. A. K. Robbins and R. A. Horlick, *BioTechniques*, 1998, **25**, 240-244.

25. J. V. Ferrer and J. A. Javitch, *Proceedings of the National Academy of Sciences*, 1998, **95**, 9238-9243.

26. N. Chen, J. V. Ferrer, J. A. Javitch and J. B. Justice, *Journal of Biological Chemistry*, 2000, **275**, 1608-1614.

27. H. Hastrup, A. Karlin and J. A. Javitch, *Proceedings of the National Academy of Sciences*, 2001, **98**, 10055-10060.

28. J. Eriksen, W. E. Bjørn-Yoshimoto, T. N. Jørgensen, A. H. Newman and U. Gether, *J Biol Chem*, 2010, **285**, 27289-27301.

29. J. Eriksen, S. G. F. Rasmussen, T. N. Rasmussen, C. B. Vaegter, J. H. Cha, M.-F. Zou, A. H. Newman and U. Gether, *The Journal of neuroscience : the official journal of the Society for Neuroscience*, 2009, **29**, 6794-6808.

30. Y. Zhou, Z. Peng, E. S. Seven and R. M. Leblanc, *Journal of Controlled Release*, 2018, **270**, 290-303.

31. C. Saraiva, C. Praça, R. Ferreira, T. Santos, L. Ferreira and L. Bernardino, *Journal of Controlled Release*, 2016, **235**, 34-47.

32. M. I. Setyawati, C. Y. Tay, S. L. Chia, S. L. Goh, W. Fang, M. J. Neo, H. C. Chong, S. M. Tan, S. C. J. Loo, K. W. Ng, J. P. Xie, C. N. Ong, N. S. Tan and D. T. Leong, *Nature Communications*, 2013, **4**, 1673.

33. F. Peng, M. I. Setyawati, J. K. Tee, X. Ding, J. Wang, M. E. Nga, H. K. Ho and D. T. Leong, *Nature Nanotechnology*, 2019, **14**, 279-286.

34. J. K. Tee, L. X. Yip, E. S. Tan, S. Santitewagun, A. Prasath, P. C. Ke, H. K. Ho and D. T. Leong, *Chemical Society Reviews*, 2019, **48**, 5381-5407.

Table 1. Physicochemical properties of NP, NP-TR, and NP-DN.

	core size (nm)	hydrodynamic size (nm)	polydispersity index	zeta potential (mV)	DN/NP	Cy5/NP
NP	8.2 ± 0.7	25.9 ± 0.59	0.084	-8.78 ± 6.4	0	0
NP-TR	8.2 ± 0.7	29.1 ± 0.97	0.181	-9.2 ± 4.7	0	2
NP-DN	8.2 ± 0.7	30.2 ± 1.3	0.238	-9.23 ± 2.7	~137	2
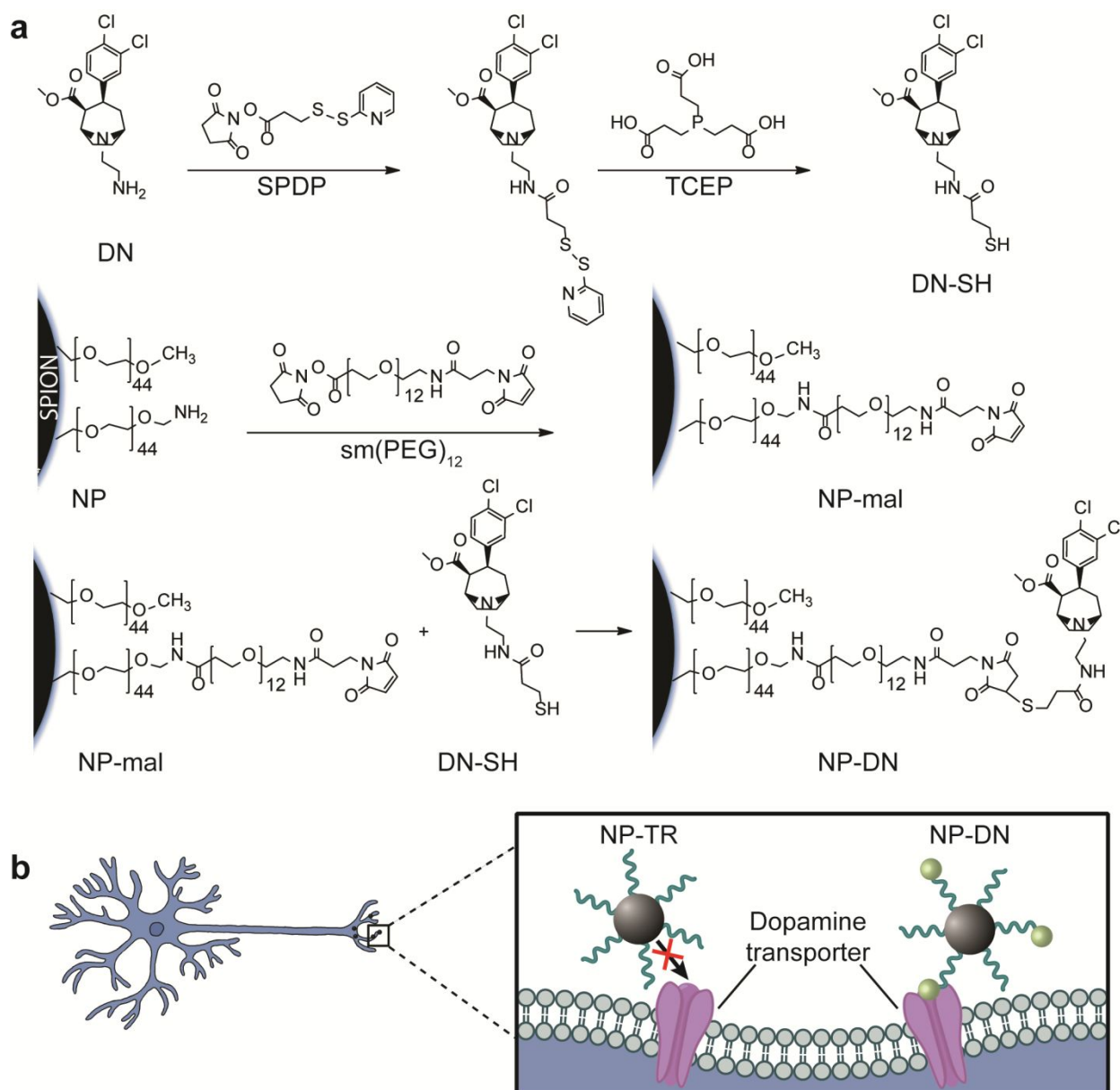
Figure 1. Illustration of synthesis of NP-DN and neuron labeling. (a) DN was modified via SPDP and TCEP to create thiolated DN-SH. Separately, NP was reacted with sm(PEG)$_{12}$ crosslinker, in

which the amine group from the NP reacted with the NHS-ester moiety of the crosslinker to form NP-mal, leaving a terminal maleimide group. The thiol group from DN-SH was then reacted with the maleimide group of the NP-mal to form NP-DN. (b) Schematic representation of DAT-mediated labeling of neurons with NP-DN.
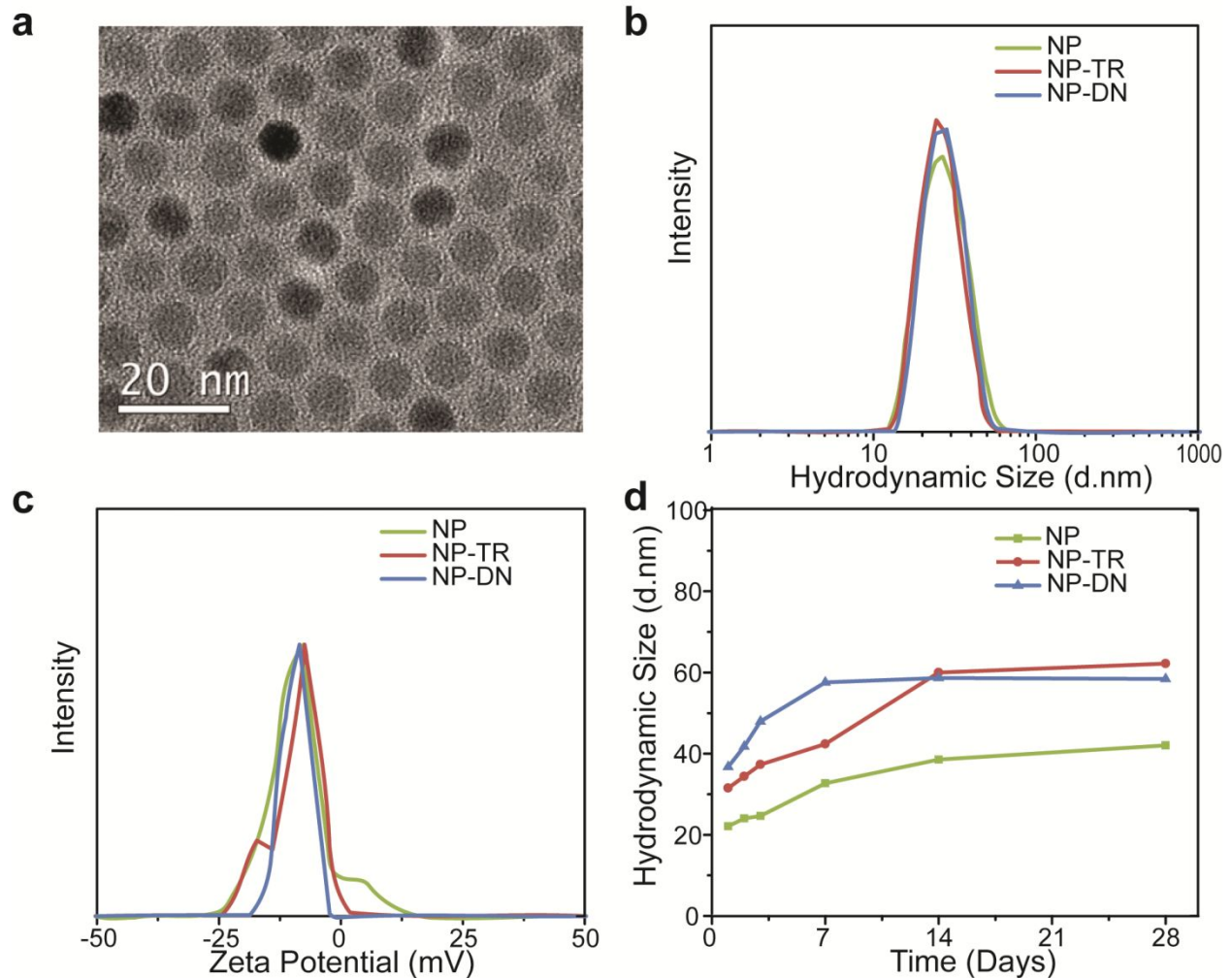
Figure 2. Physical properties of NPs. (a) TEM images of NPs. (b) Hydrodynamic size distributions and (c) Zeta potential distributions of NP (purple), NP-TR (red), and NP-DN (blue). (d) Hydrodynamic sizes of NP (purple), NP-TR (red), and NP-DN (blue) in cell culture media at 37°C as a function of time for a period of 28 days.
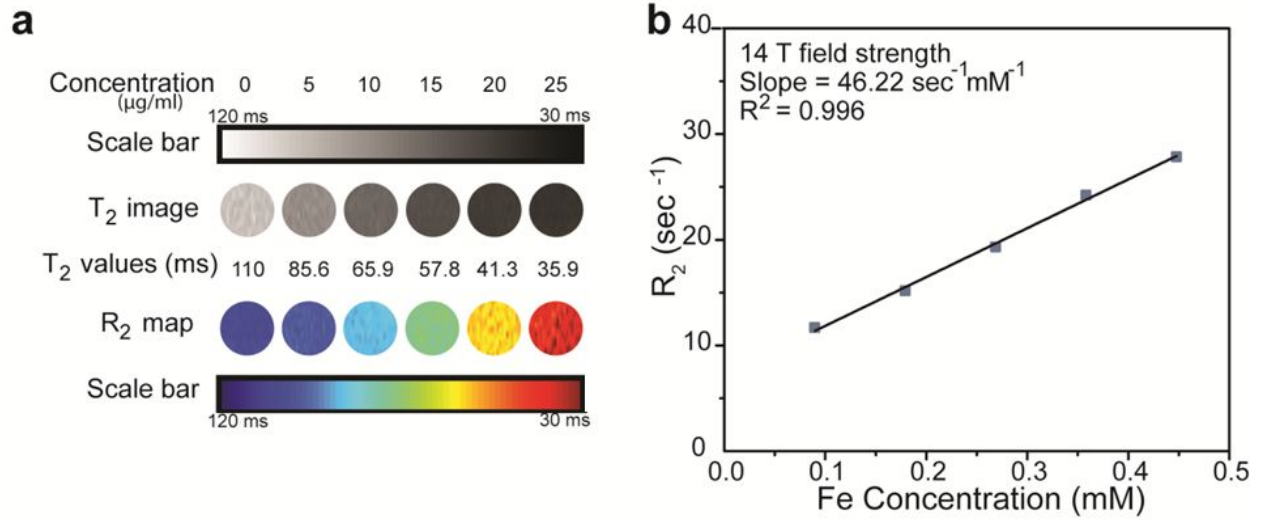
Figure 3. Magnetic properties of NP-DN. (a) T_2-weighted MR images and R_2 maps of NP-DN at various Fe concentrations. (b) Plot of R_2 as a function of Fe concentration. The slope of the fitted linear line gives the specific relaxivity of r_2.
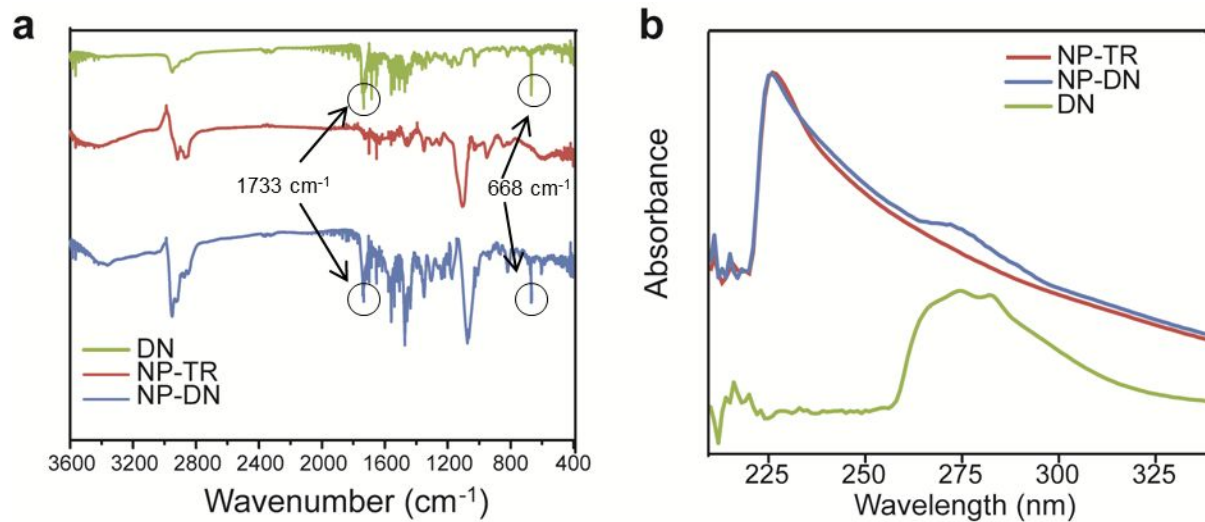
Figure 4. Chemical analysis of NP-DN. (a) FTIR spectra of DN (green), NP-TR (red), and NP-DN (blue). (b) UV-vis spectra of NP-TR (red), NP-DN (blue), and DN (green). The DN ligand exhibits a broad peak around 275 nm, which corresponds to the shoulder peak of NP-DN spectrum.
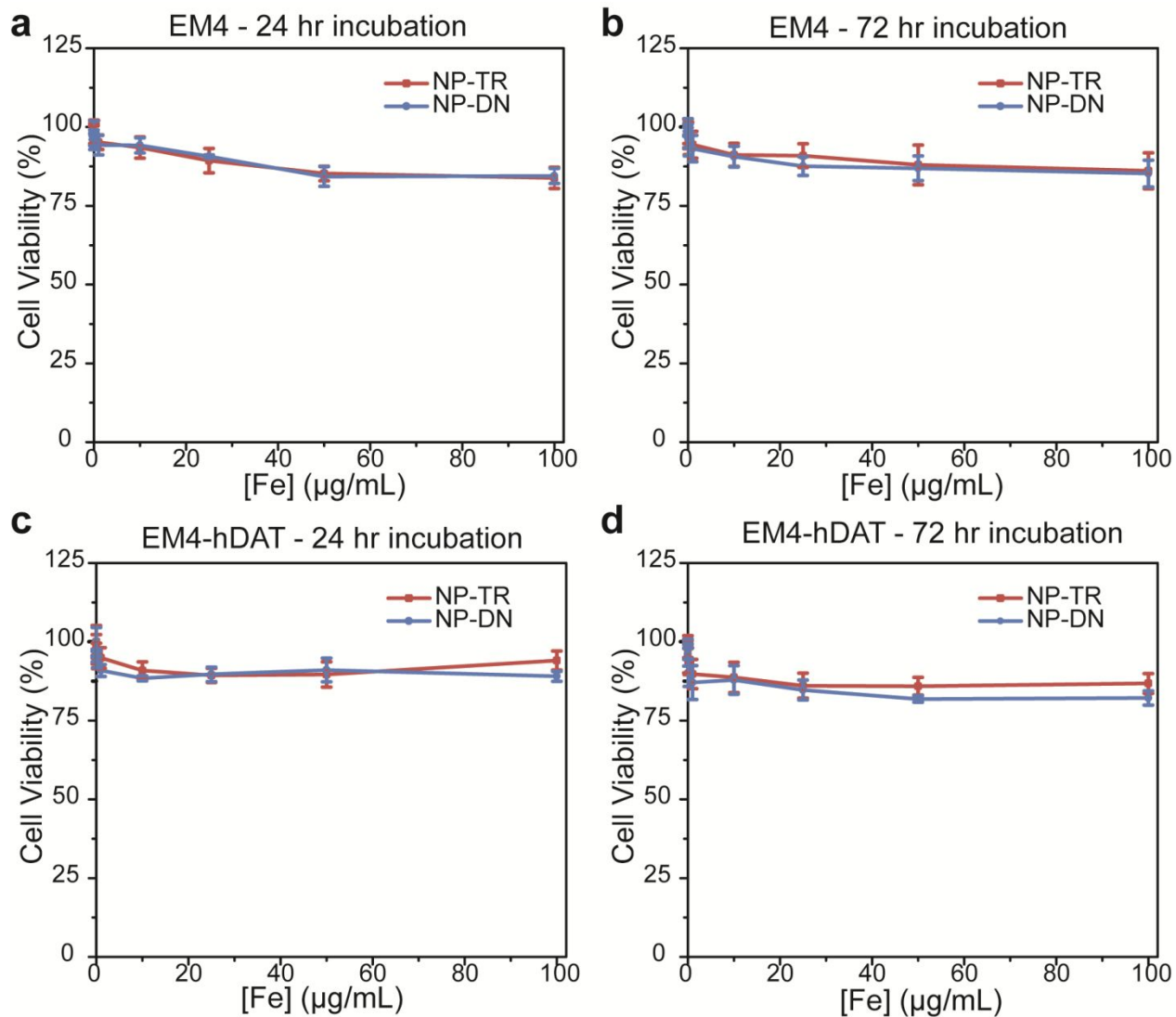
Figure 5. Viability of EM4 (DAT⁻) and EM4-hDAT (DAT⁺) cells treated with NP-TR and NP-DN. (a-b) Cell viability of EM4 cells as a function of Fe concentration after incubation for (a) 24 hours or (b) 72 hours with NP-TR (red) or NP-DN (blue) in cell culture media. (c-d) Cell viability of EM4-hDAT cells as a function of Fe concentration after incubation for (a) 24 hours or (b) 72 hours with NP-TR (red) or NP-DN (blue) in cell culture media.
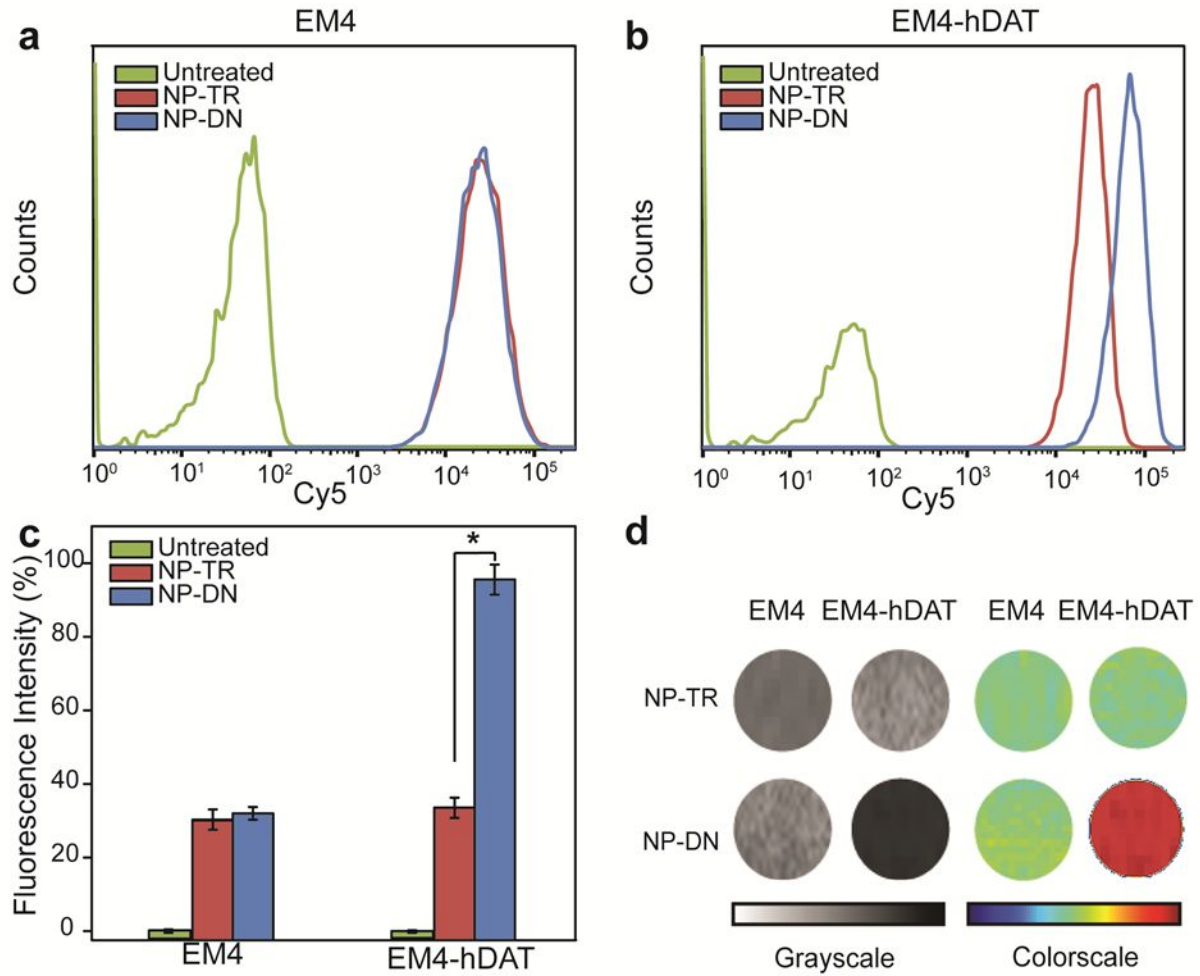
Figure 6. Flow cytometry analysis and phantom MR analysis of NP-DN targeting of DAT expressing cells. Cellular labeling of NP-TR (red) and NP-DN (blue) on (a) EM4 (DAT$^-$) and (b) EM4-hDAT (DAT$^+$). (c) Quantitative mean fluorescence intensities of NP-TR and NP-DN from flow analysis (* $p < 0.0005$). (d) T$_2$-weighted and R$_2$-mapped images of NP-TR and NP-DN on EM4 and EM4-hDAT cells.
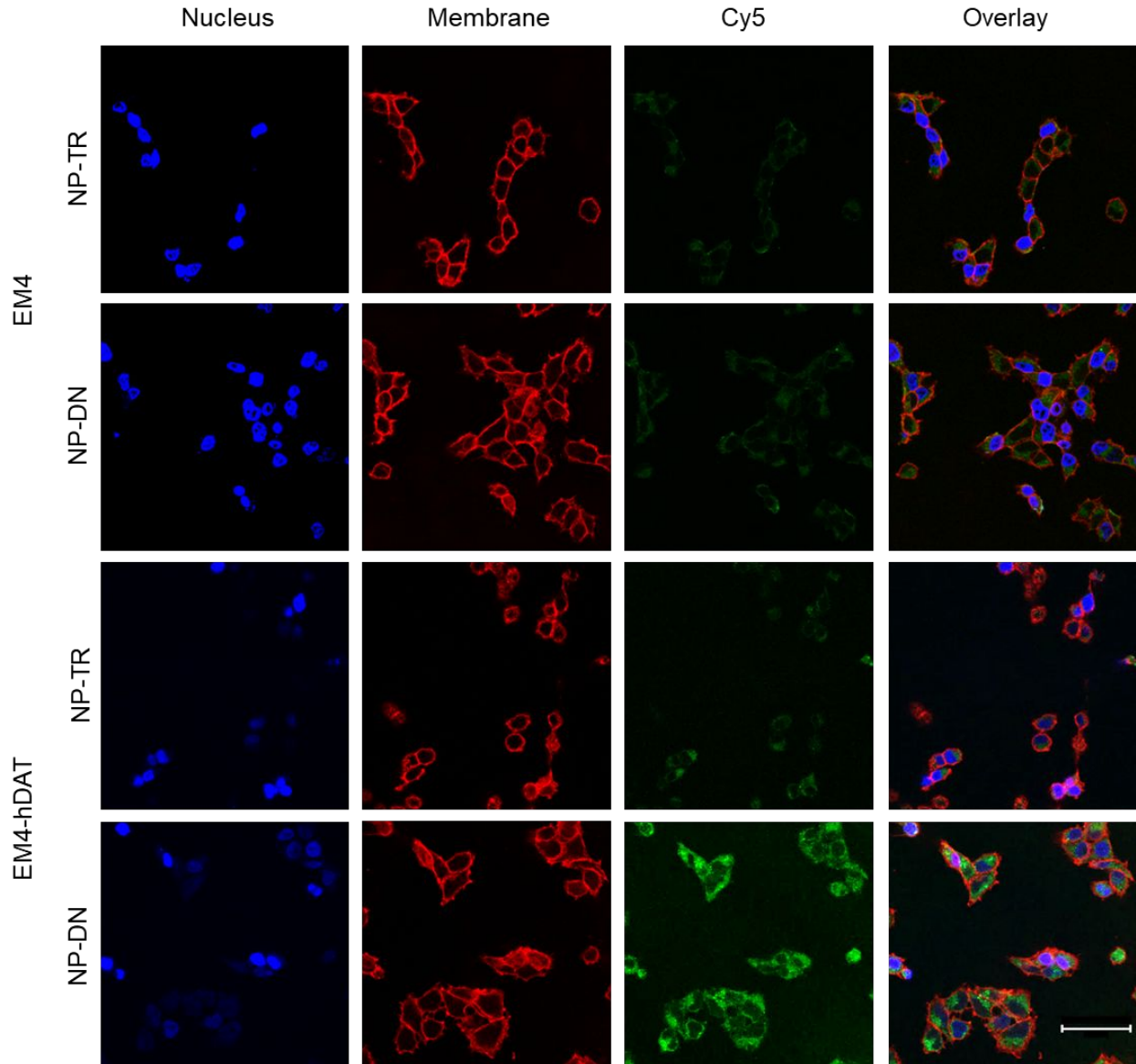
Figure 7. Confocal fluorescence images of EM4 (DAT⁻) and EM4-hDAT (DAT⁺) cells treated with either NP-TR or NP-DN. EM4 cells (top two rows) and EM4-hDAT (bottom two rows) were treated for 2 hours with either NP-TR or NP-DN. The first column shows nuclei stained in blue, the second column shows the membrane stained in red, and the third column shows the fluorescent NP-TR and NP-DN in green, and the fourth column shows the overlay of the first three columns. The scale bar corresponds to 50 μm.

Table of Contents

A magnetic nanoparticle, composed of an iron oxide core with a polyethylene glycol coating conjugated with a cocaine analogue, exhibits small particle size and long-term stability with the ability to specifically target dopamine transporter-expressing neurons while providing excellent contrast enhancement under MRI, demonstrating great potential for neuroimaging.

Keywords: dopamine transporter, magnetic nanoparticles, neurons, neuroimaging

Cocaine Analogue Conjugated Magnetic Nanoparticles for Labeling and Imaging Dopaminergic Neurons